

Supporting Information

Semiconducting and environmental-responsive melanin-doped silk nanofibres for multifunctional electronic tattoos

Shalik Ram Joshi,^a Soohoon Lee,^a and Sunghwan Kim^{*,a,b}

^aDepartment of Electronic Engineering, Hanyang University, Seoul Campus, South Korea

^bDepartment of Biomedical Engineering, Hanyang University, Seoul Campus, South Korea

*Corresponding author: (skim81@hanyang.ac.kr) (S. Kim)

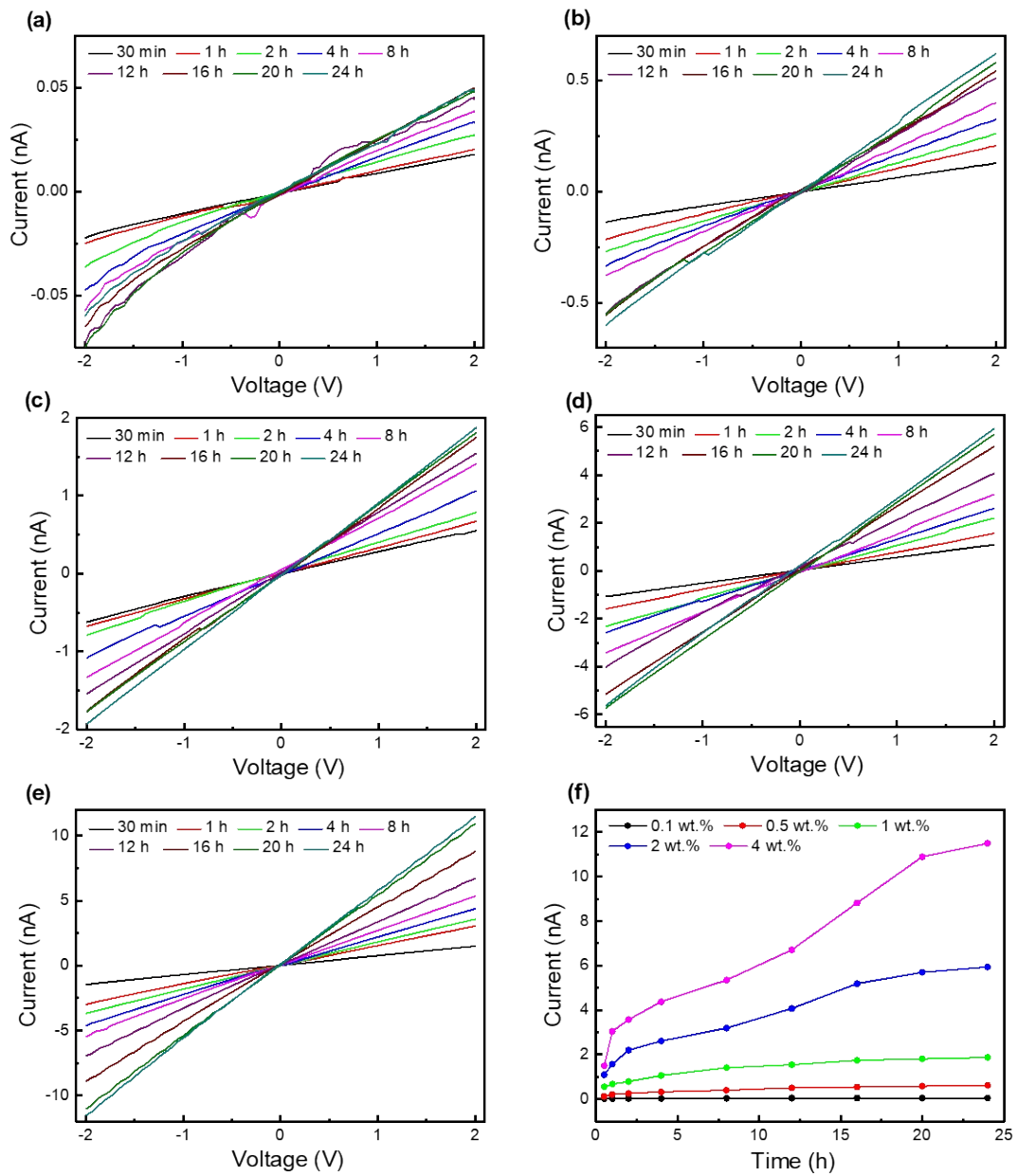


Fig. S1. Variation in the I-V curve due to the change in the immersion time for **(a)** 0.1 wt.%, **(b)** 0.5 wt.%, **(c)** 1 wt.%, **(d)** 2 wt.%, and **(e)** 4 wt.% melanin-doped-SNF mat. The dimension of the melanin-doped-SNF mat was kept at 1 cm x 1 cm. **(f)** Change in current (@ 2V) due to the change in the immersion time with melanin concentration.

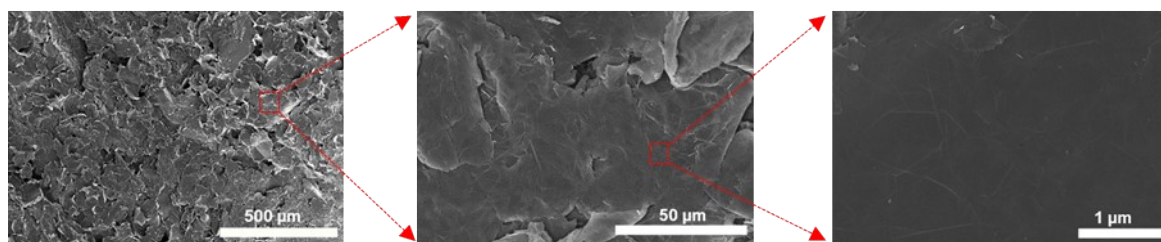


Fig. S2. Scanning electron microscopy (SEM) images at different length scales showing the uniform coating of graphene on melanin-doped-SNF.

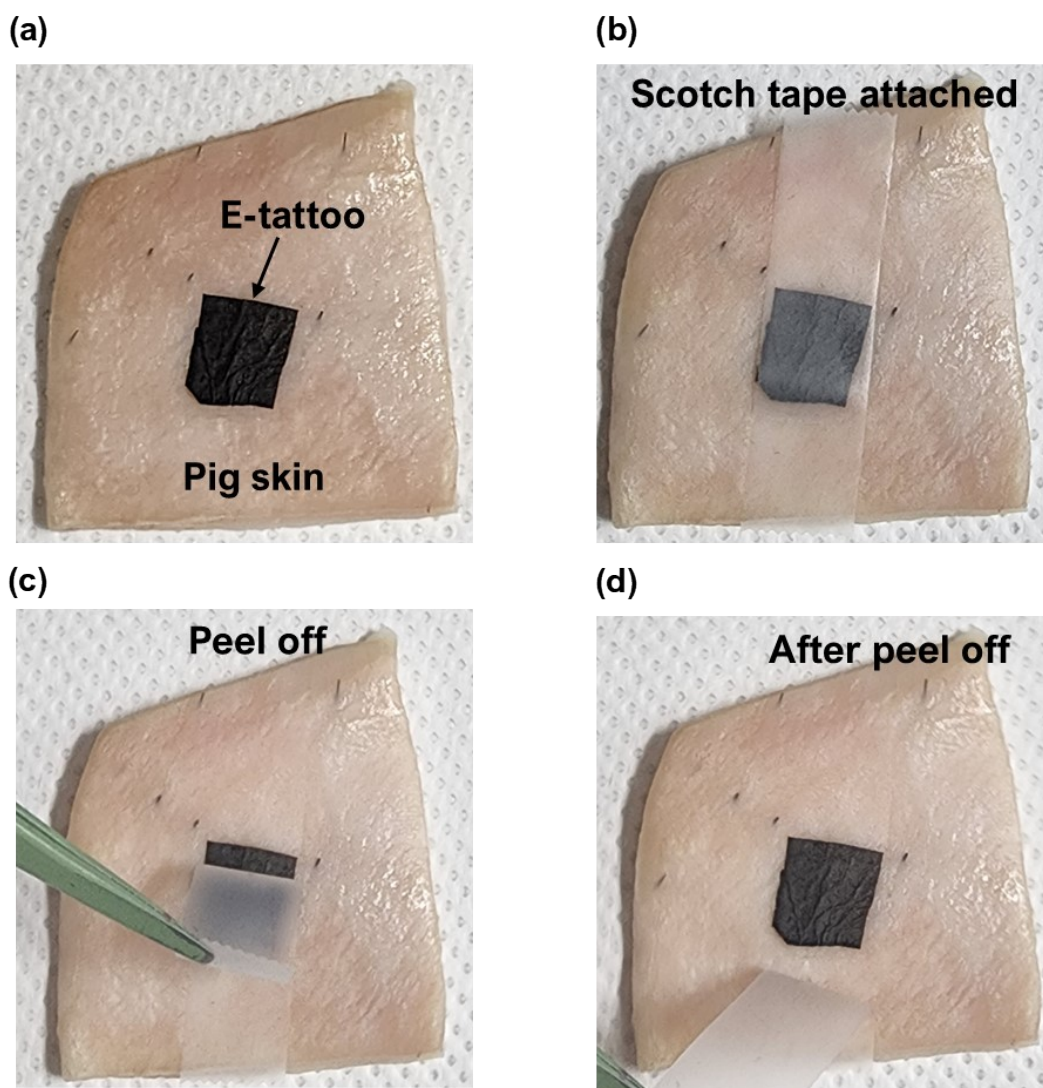


Fig. S3. Optical images showing the E-tattoo **(a)** initially attached to pig skin, **(b)** after applying scotch tape over the E-tattoo, **(c)** during the peeling-off process, and **(d)** following complete removal of the tape, confirming the strong and stable adhesion of the E-tattoo to the skin surface.

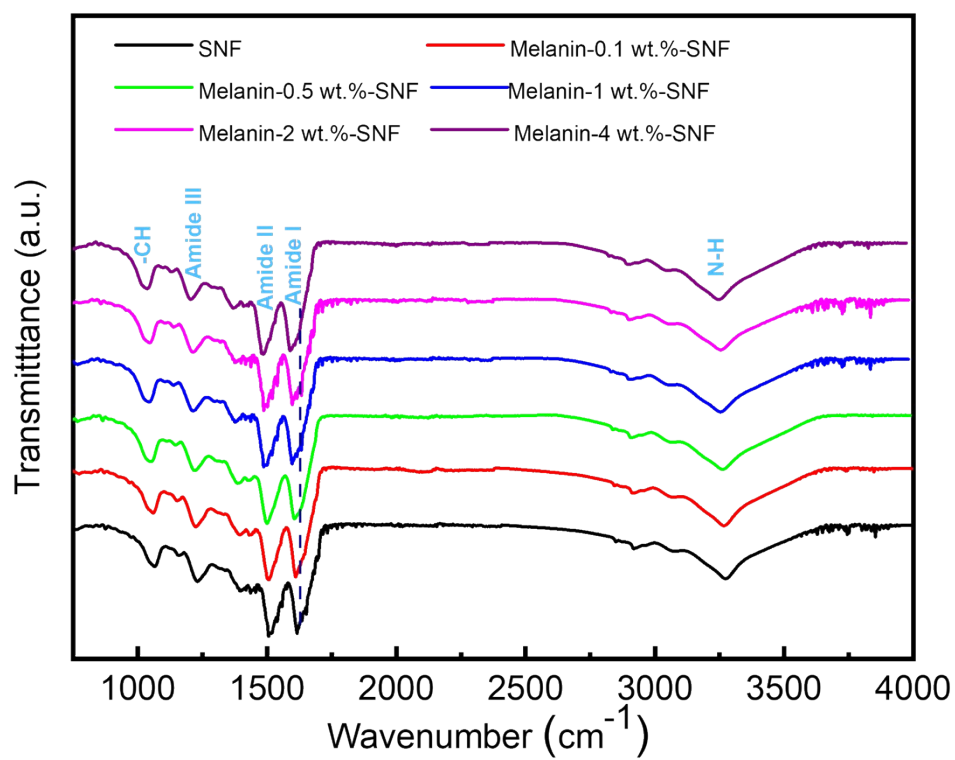


Fig. S4. FT IR spectra of the melanin-doped-SNF mat with increased melanin concentration.

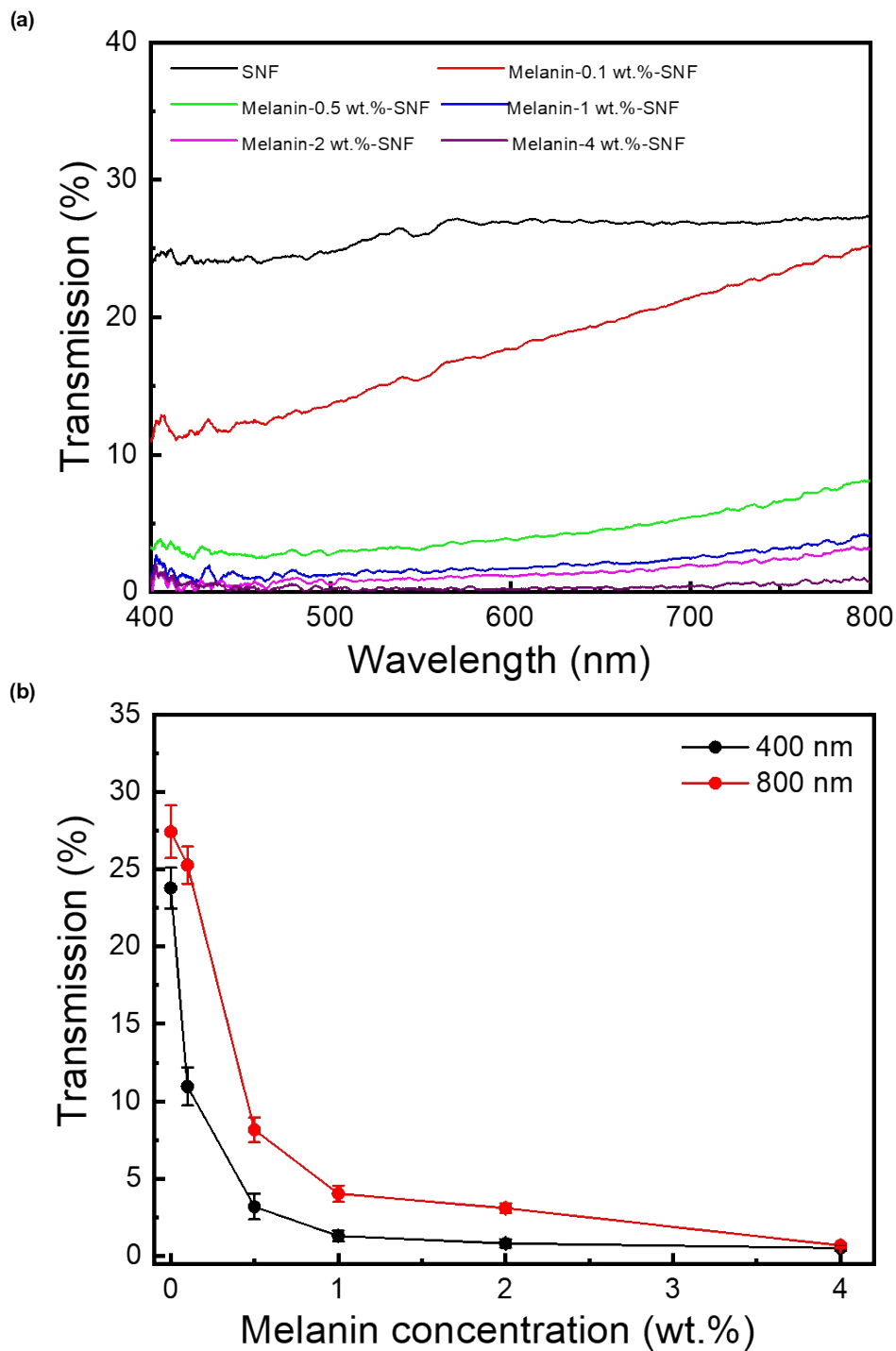


Fig. S5. (a) Optical transmission spectra of the melanin-doped-SNF mat with increased melanin concentration. (b) Percentage of optical transmission at 400 nm (visible region) and 800 nm (NIR region) with increased melanin concentration.

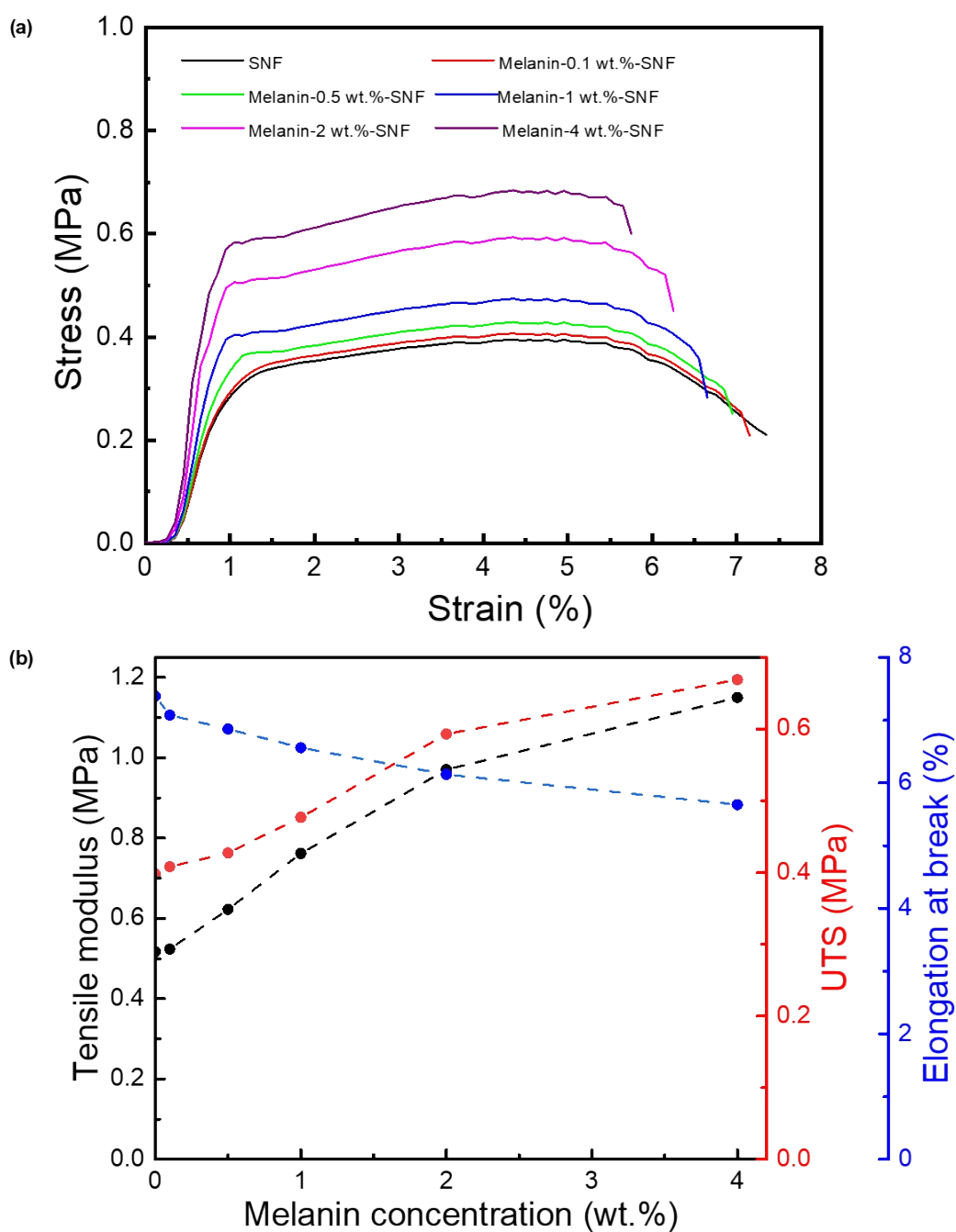


Fig. S6. (a) Stress-strain curve of the melanin-doped-SNF mat with increase in the melanin concentration. **(b)** Variation in Tensile modulus, ultimate tensile strength (UTS), and elongation at break percentage with increase in melanin concentration in SNF Mat.

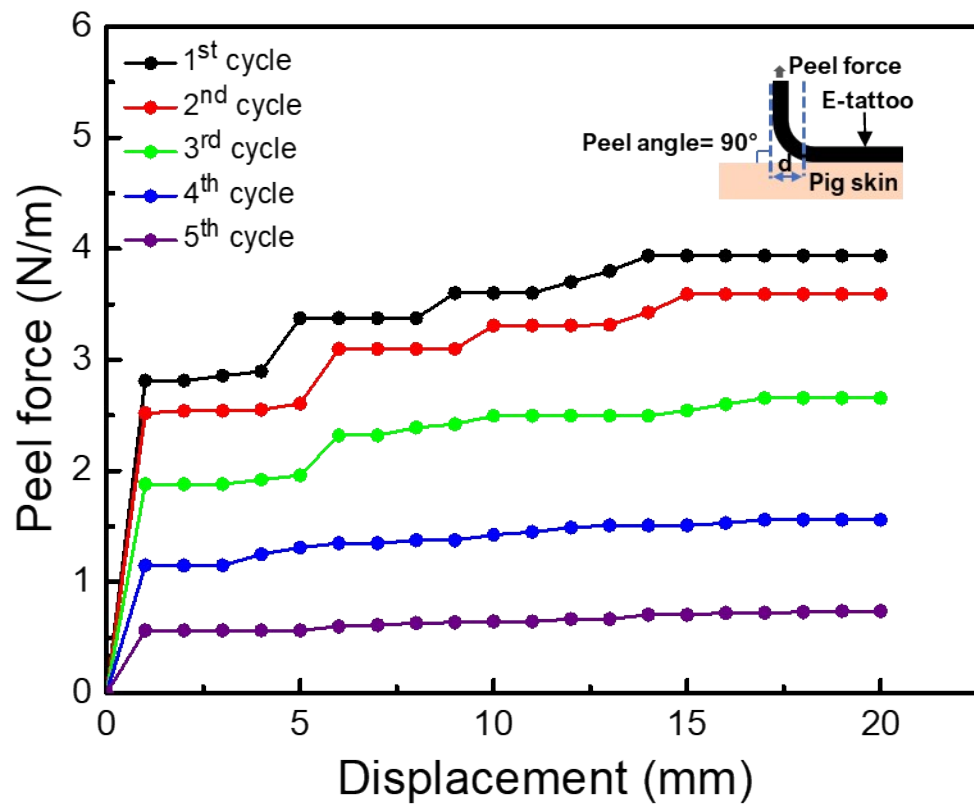


Fig. S7. Skin adhesion properties of the E-tattoo platform for five consecutive peeling-unpeeling cycles. Inset shows the peel-test geometry.

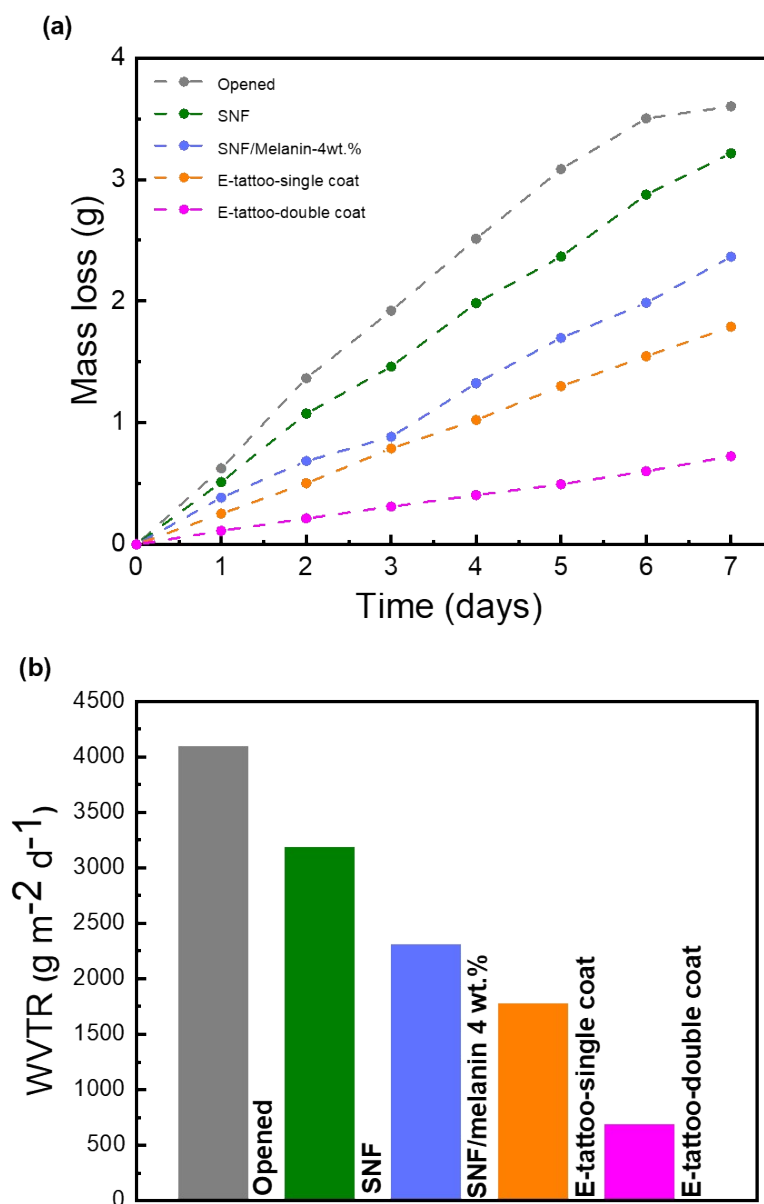


Fig. S8. (a) Water loss over time and (b) comparison of the water vapor transmission rate (WVTR) of the E-tattoo platform with a melanin-doped SNF mat for single and double graphene coatings, highlighting the impact of graphene layers on breathability.

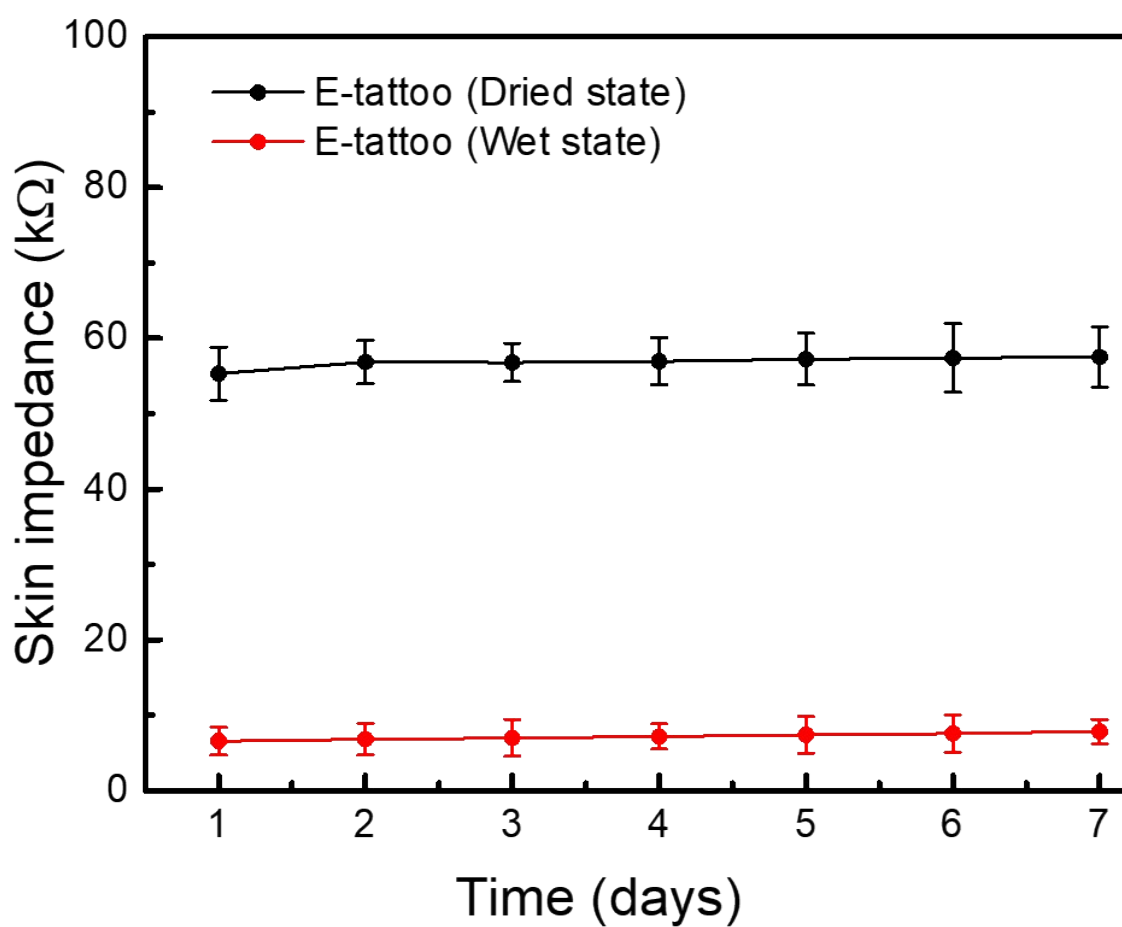


Fig. S9. Long-term stability of the pigskin impedance at 100 Hz frequency using the Graphene/Melanin-doped-SNF E-tattoo platform.

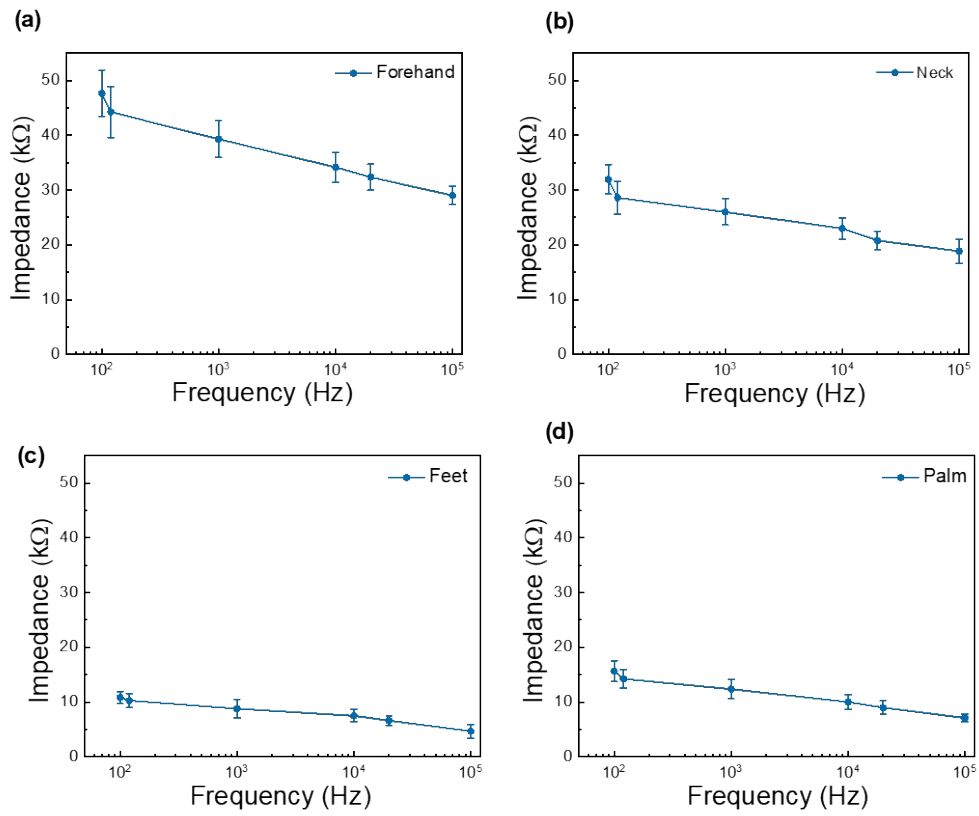


Fig. S10. Impedance measurement across (a) forehand, (b) neck, (c) feet, and (d) palm of the human body using E-tattoo platform

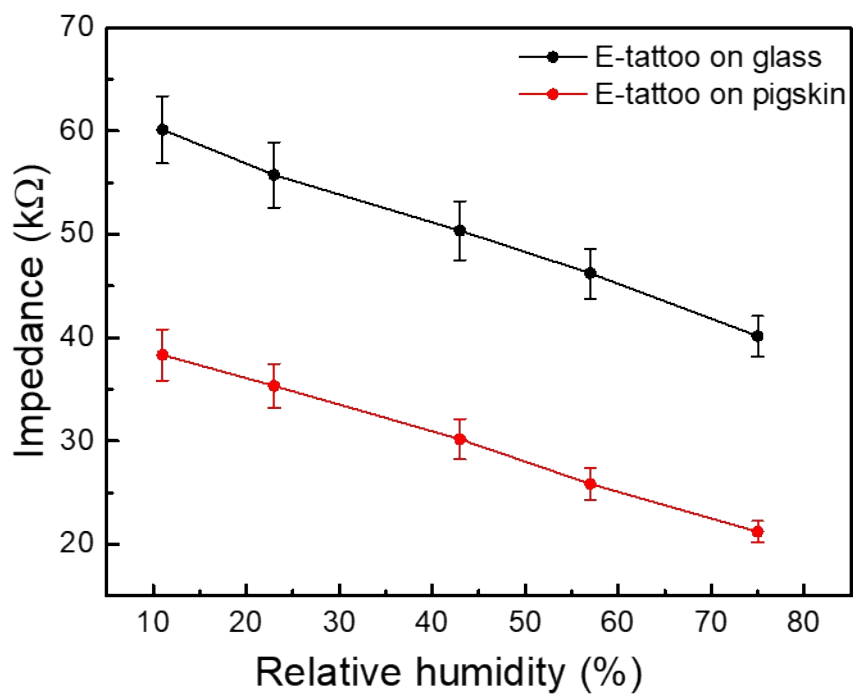


Fig. S11. Impedance measurement at 100 Hz across various humidity levels (%RH) for estimating the calibration correction. The E-tattoo platform was placed on both a glass slide (dry condition) and pigskin (maintained at 40% RH moisture level).

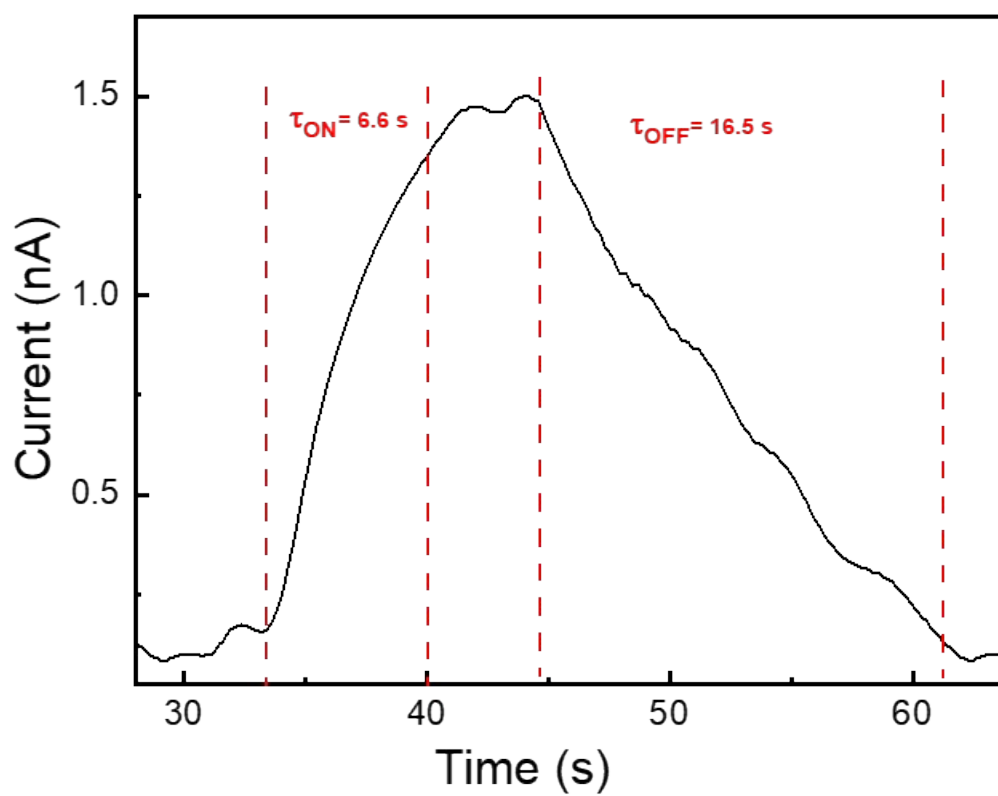


Fig. S12. Response and Recovery time of the melanin-doped-SNF mat when UV LED was ON and OFF, respectively.

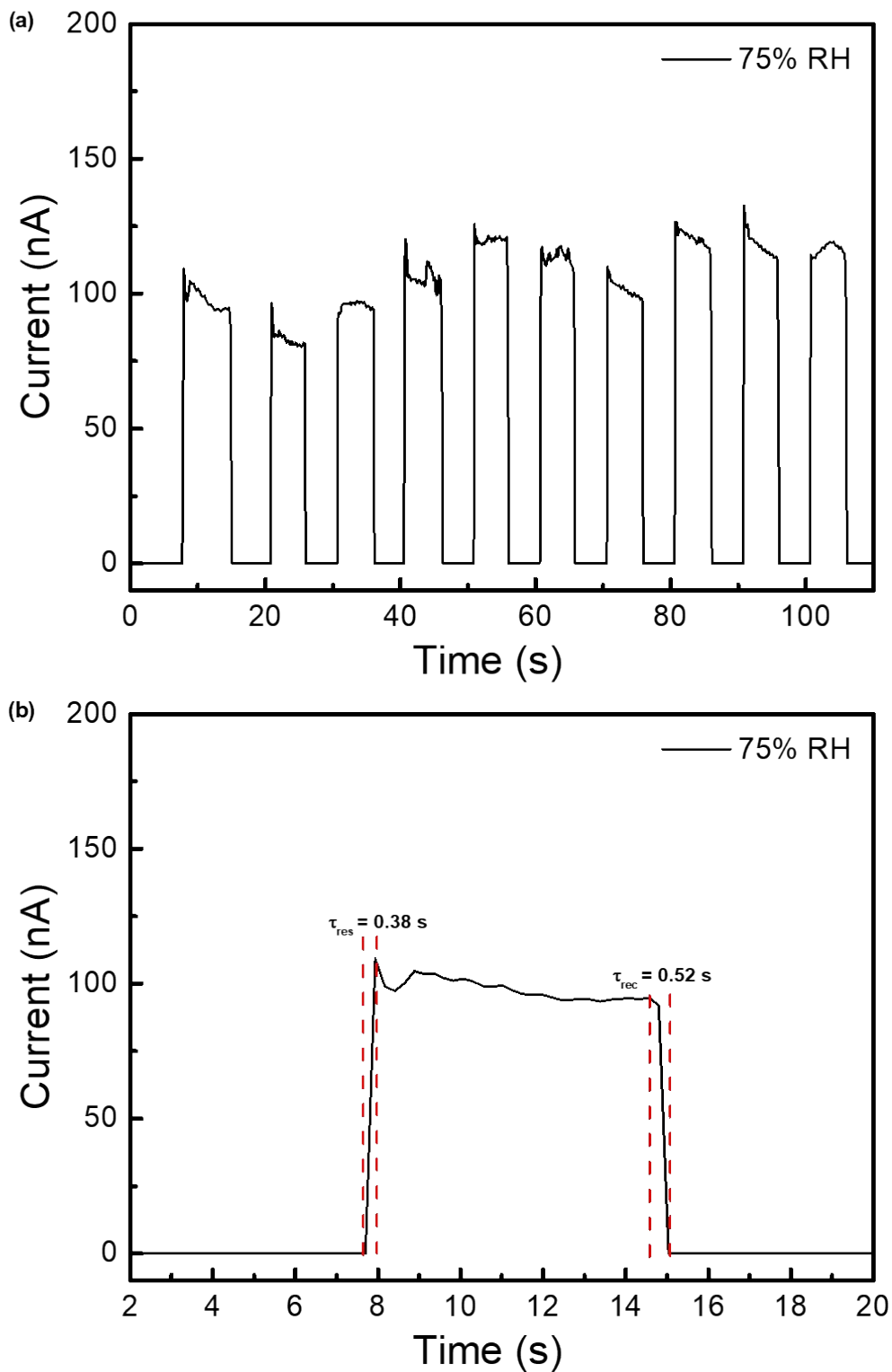


Fig. S13. (a) Response curves for repeated cycles of humidity change between 2 and 75% RH measured using Melanin-doped-SNF-based humidity sensor. **(b)** Response and Recovery time of the sensor.

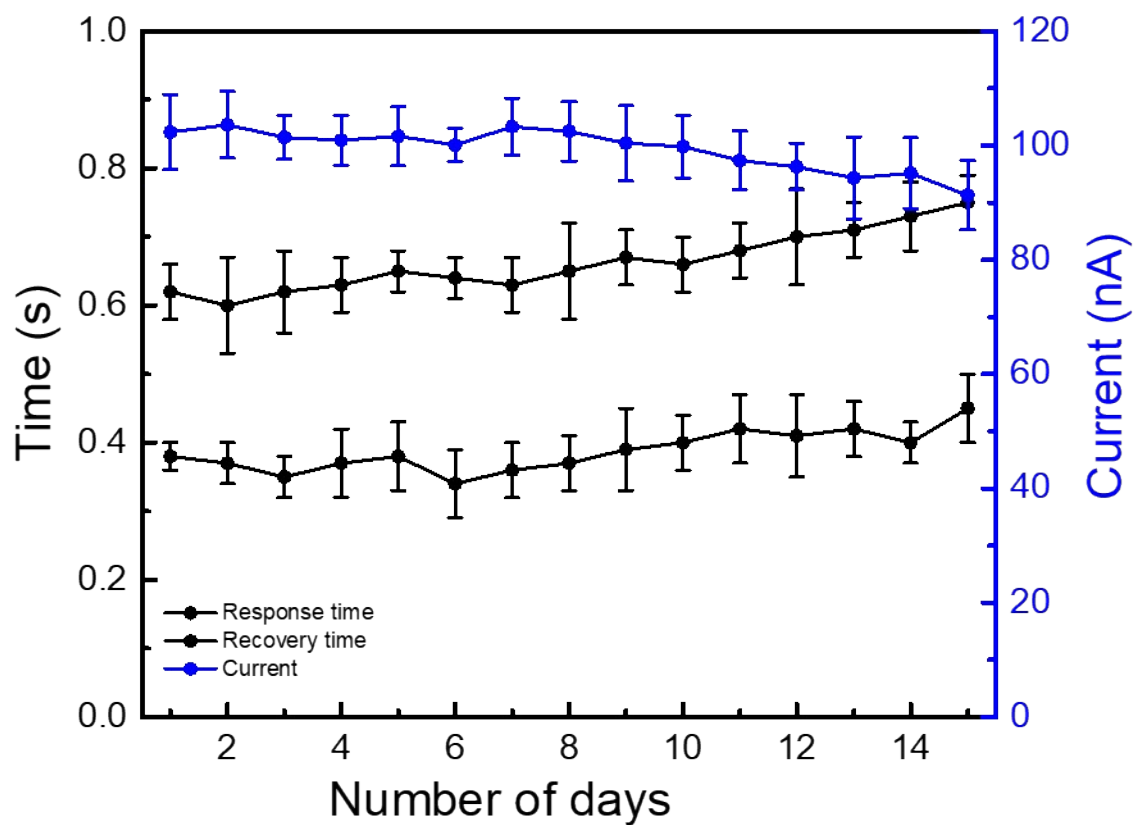


Fig. S14. Long-term stability of the melanin-doped SNF based humidity sensor results in terms of current response and response/recovery times for 75% RH.

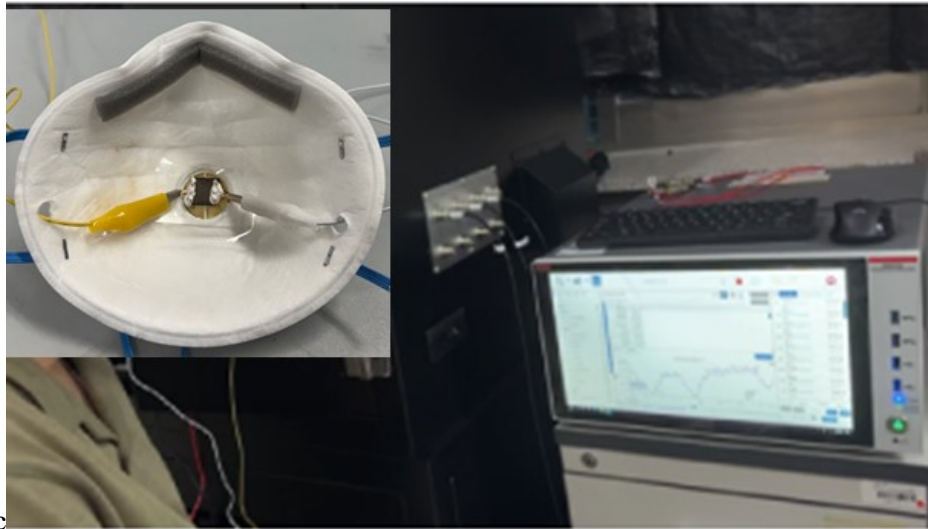


Fig. S15. Optical photograph showing the Melanin-doped-SNF-based humidity sensor attached to the Facemask.

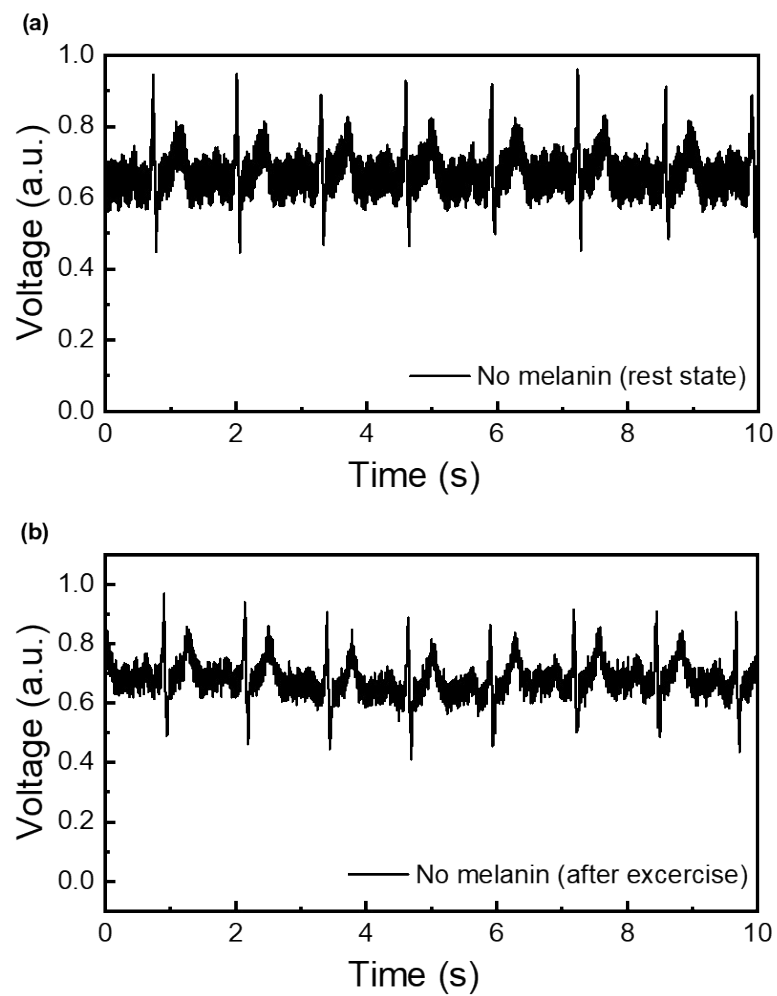


Fig. S16. ECG signals recorded using E-tattoo without melanin-doped during **(a)** rest state and **(b)** post-physical activity.

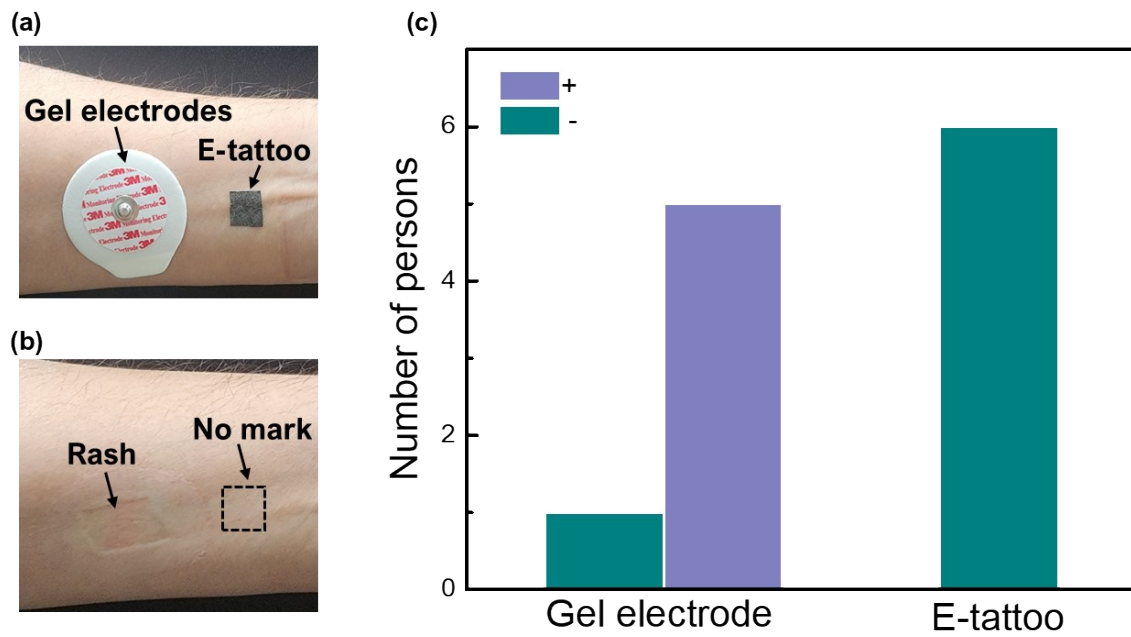


Fig. S17. (a) Comparison of skin irritation after a 24-h application of an E-tattoo and a gel electrode on the human forearm. (b) Optical image of the forearm following the removal of electrodes after 24 h. (c) Assessment of dermatitis symptoms after prolonged electrode attachment, where "+" denotes individuals who developed rashes, and "-" represents those without skin irritation.

Table S1: Comparison of Water Vapor Transmission Rate (WVTR) for the E-tattoo Platform with previously reported fiber-based platform.

| S.no | Sample details | Thickness | WVTR | Ref |
|-------------|--------------------------------------|------------------------------------|--|----------------------|
| 1. | Graphene based E-tattoo | 10 μm | 2770 $\text{g m}^{-2} \text{d}^{-1}$ | [1] |
| 2. | AgNw/PU nanofiber | 20 μm | 2304 $\text{g m}^{-2} \text{d}^{-1}$ | [2] |
| 3. | Copper coated conductive fabric | 80 μm | 1500 $\text{g m}^{-2} \text{d}^{-1}$ | [3] |
| 4. | Liquid metal fiber mat | 320 μm | 520 $\text{g m}^{-2} \text{d}^{-1}$ | [4] |
| 5. | CNT/Cotton fabric | NA | 1200 $\text{g m}^{-2} \text{d}^{-1}$ | [5] |
| 6. | Graphene/Melanin-SNF E-tattoo | 30 μm | 1783 $\text{g m}^{-2} \text{d}^{-1}$ | Present study |

Table S2. Performance comparison of Melanin-doped-SNF-based UV-photodetector with previously reported nanofiber-based photodetectors.

| Device structure | Type | Flexibility | Response | τ_{ON}/τ_{OFF} [s] | Ref |
|-------------------------------------|------------------|--------------------|-----------------|--|----------------------|
| Zn/ZnO NRAs/PVK/PEDOT:PSS | Nanofiber | Low | 1.5 | 6/7 | [6] |
| CNT/ZnO NRAs/CdS/ITO | Nanofiber | Low | 7.2 | 10/30 | [7] |
| Zn/ZnO NRAs/PVK/PEDOT:PSS/CNT fiber | Nanofiber | Low | 2 | 1.5/6 | [8] |
| Ni/ZnO/ZnO NWs/ | Nanofiber | Low | 4 | 7.5/8.6 | [9] |
| Ni/NiO/ZnO NRAs/ | Nanofiber | Low | 4.9 | 10/18.1 | [10] |
| Co 3O ₄ /graphene | Nanofiber | Low | 2.5 | 18/17 | [11] |
| Melanin-SNF | Nanofiber | High | 21.4 | 6.5/16.5 | Present study |

Table S3. Performance comparison of Melanin-doped-SNF-based humidity sensor with previously reported nanofiber-based photodetectors.

| Device structure | Device type | τ_{ON}/τ_{OFF} [s] | Ref |
|-------------------------|--------------------|--|----------------------|
| PANI-PSSA/PEO/PV | Impedance | 8/6 | [12] |
| PVA/Parylene/Au | Resistance | 148/110 | [13] |
| ZnO/TiO ₂ | Impedance | 11/7 | [14] |
| PEDOT-PSS/PVA | Frequency | 5.9/3.5 | [15] |
| SPEEK/PVB | Impedance | 1/5 | [16] |
| SnO ₂ @G-GO | Impedance | 1/1 | [17] |
| Melanin-SNF | Resistance | 0.38/0.52 | Present study |

Appendix-A

Calibration equation of E-tattoo platform for skin hydration monitoring sensor

As the data (Fig. S11) shows the linear trend, we utilized the linear regression analysis, assuming the independent variable as relative humidity (RH) and dependent variable as impedance (Z).

We assume the linear relationship of the form

$$RH = mZ + c \quad \#(1)$$

Where m is the slope and c is the intercept. These values can be obtained using the following regression formula

$$m = \frac{N \sum (X_i Y_i) - \sum X_i \sum Y_i}{N \sum X_i^2 - (\sum X_i \times \sum X_i)} \quad \#(2)$$

$$c = \frac{\sum Y_i - m \sum X_i}{N} \quad \#(3)$$

Where, N is the number of data points, X_i is the humidity values, and Y_i is the impedance values.

Thus, using the above equation, we can obtain the linear regression equation.

$$RH = -3.274 \times Z + 207.2 \quad \#(4)$$

Now to obtain the corrected skin impedance, firstly we estimated the correct skin impedance using the following formula

$$Z_{skin, corrected} = \frac{Z_{skin, measured}}{Z_{dry, predicted}} \quad \#(5)$$

$$Z_{skin,corrected} = Z_{skin,measured} \times \left(\frac{3.274}{207.2 - RH} \right) \#(6)$$

Where, $Z_{skin,corrected}$ is the true skin impedance after removing environmental effects, $Z_{skin,measured}$ is the impedance measured using our E-tattoo platform, and RH is the ambient humidity in %.

References

- [1] D. Kireev, J. Kampfe, A. Hall and D. Akinwande, *NPJ 2D Mater.*, 2022, **46**, 1.
- [2] Z. Jiang, M. O. G. Nayeem, K. Fujuda, S. Ding, H. Jin, T. Yokota, D. Inoue, D. Hashizume and T. Someya, *Adv. Mater.*, 2019, **31**, 1903446.
- [3] Z. Liu, Y. Zheng, L. Jin, K. Chen, H. Zhai, Q. Huang, Z. Chen, Y. Yi, M. Umar, L. Xu, G. Li, Q. Song, P. Yue, Y. Li and Z. Zheng, *Adv. Funct. Mater.*, 2021, **31**, 2007622.
- [4] Z. Ma, Q. Huang, Q. Xu, Q. Zhuang, X. Zhao, Y. Yang, H. Qiu, Z. Yang, C. Wang, Y. Chai and Z. Zheng, *Nat. Mater.*, 2021, **20**, 859.
- [5] X. Zhang, L. Ke, X. Zhang, F. Xu, Y. Hu, H. Lin and J. Zhu, *ACS Appl. Mater. Interfaces*, 2022, **14**, 25753.
- [6] Z. Zhu, D. Ju, Y. Zou, Y. Dong, L. Luo, T. Zhang, D. Shan and H. Zeng, *ACS Appl. Mater. Interfaces*, 2017, **9**, 12092.
- [7] F. Zhang, S. M. Niu, W. X. Guo, G. Zhu, Y. Liu, X. L. Zhang and Z. L. Wang, *ACS Nano*, 2013, **7**, 4537.
- [8] Y. Dong, Y. Zou, J. Song, Z. Zhu, J. Li and H. Zeng, *Nano Energy*, 2016, **30**, 173.

- [9] Y. H. Ko, G. Nagaraju and J. S. Yu, *Nanoscale*, 2015, **7**, 2735.
- [10] J. Chen, L. Ding, X. Zhang, L. Chu, N. Liu and Y. Gao, *Opt. Expr.*, 2014, **22**, 3661.
- [11] X. Wang, B. Liu, R. Liu, Q. Wang, X. Hou, D. Chen, R. Wang and G. Shen, *Ang. Chem.*, 2014, **53**, 1849
- [12] Q. Lin, Y. Li and M. Yang, *Sens. Actuators B*, 2012, **161**, 967–972.
- [13] W. Jeong, J. Song, J. Bae, K. R. Nandanapalli and S. Lee, *ACS Appl. Mater. Interfaces*, 2019, **11**, 44758–44763.
- [14] X. J. Yue, T. S. Hong, X. Xu and Z. Li, *Chin. Phys. Lett.*, 2011, **28**, 090701.
- [15] T. Julian, A. Rianjanu, S. N. Hidayat, A. Kusumaatmaja, R. Roto and K. Triyana, *J. Sens. Sens. Sys.*, 2019, **8**, 243–250.
- [16] X. Li, Z. Zhuang, D. Qi and C. Zhao, *Sens. Actuators B*, 2021, **330**, 129239
- [17] J. Xu, S. Gu and B. Lu, *RSC Adv.*, 2015, **5**, 72046–72050.

